

# Experimental study of emergent ground state behavior in $\text{Gd}_{1-x}\text{Ce}_x\text{Ni}_5$ ( $x = 0; 0.2; 0.5; 0.8$ and 1) melt-spun ribbons

Cite as: AIP Advances 12, 035226 (2022); <https://doi.org/10.1063/9.0000277>

Submitted: 30 October 2021 • Accepted: 05 December 2021 • Published Online: 14 March 2022

 Andrea Dzubinska, Jesús Rodríguez Fernández, Marian Reiffers, et al.

## COLLECTIONS

Paper published as part of the special topic on [15th Joint MMM-Intermag Conference](#)



View Online



Export Citation



CrossMark

## ARTICLES YOU MAY BE INTERESTED IN

[Near room temperature magnetocaloric properties in Ni deficient  \$\(\text{Mn}\_{0.525}\text{Fe}\_{0.5}\)\text{Ni}\_{0.975}\text{Si}\_{0.95}\text{Al}\_{0.05}\$](#)

AIP Advances 12, 035227 (2022); <https://doi.org/10.1063/9.0000294>

[Domain wall propagation in Fe-rich magnetic microwires with graded magnetic anisotropy](#)

AIP Advances 12, 035228 (2022); <https://doi.org/10.1063/9.0000324>

[Critical behavior of the classical spin-1 Ising model for magnetic systems](#)

AIP Advances 12, 035326 (2022); <https://doi.org/10.1063/9.0000288>



# Experimental study of emergent ground state behavior in $\text{Gd}_{1-x}\text{Ce}_x\text{Ni}_5$ ( $x = 0; 0.2; 0.5; 0.8$ and $1$ ) melt-spun ribbons

Cite as: AIP Advances 12, 035226 (2022); doi: 10.1063/9.0000277

Presented: 27 December 2021 • Submitted: 30 October 2021 •

Accepted: 5 December 2021 • Published Online: 14 March 2022



View Online



Export Citation



CrossMark

Andrea Dzubinska,<sup>1,a)</sup>  Jesús Rodríguez Fernández,<sup>2</sup> Marian Reiffers,<sup>3</sup> Jose Ignacio Espeso,<sup>2</sup> Rastislav Varga,<sup>1</sup> K. Arun,<sup>4</sup> and Jose Carlos Gómez Sal<sup>2</sup>

## AFFILIATIONS

<sup>1</sup> CPM-TIP, University of Pavol Jozef Safarik, Tr. SNP 1, 040 11 Kosice, Slovakia

<sup>2</sup> CITIMAC, University of Cantabria, Av. de los Castros s/n, 390 05 Santander, Spain

<sup>3</sup> Faculty of Humanities and Natural Sciences, University of Presov, Ul. 17. novembra 1, 080 01 Presov, Slovakia

<sup>4</sup> Department of Physics, National Institute of Technology, 620 015 Tiruchirappalli, India

**Note:** This paper was presented at the 15th Joint MMM-Intermag Conference.

<sup>a)</sup> Author to whom correspondence should be addressed: [andrea.dzubinska@upjs.sk](mailto:andrea.dzubinska@upjs.sk)

## ABSTRACT

The ground state physical properties of  $\text{Gd}_{1-x}\text{Ce}_x\text{Ni}_5$  ( $x = 0; 0.2; 0.5; 0.8$  and  $1$ ) melt-spun ribbons were investigated by X-ray diffraction, magnetization and specific heat measurements. The produced ribbon samples are single phases with the hexagonal  $\text{CaCu}_5$ -type crystal structure. The magnetic transition temperature decreases with increasing Ce content. At a temperature around 100 K for the  $\text{CeNi}_5$  melt-spun ribbon, the spin fluctuations effect is visible.

© 2022 Author(s). All article content, except where otherwise noted, is licensed under a Creative Commons Attribution (CC BY) license (<http://creativecommons.org/licenses/by/4.0/>). <https://doi.org/10.1063/9.0000277>

## I. INTRODUCTIONS

For more than five decades, rare earth intermetallic compounds have been investigated and studied because of their interesting physical properties. All compounds from the  $\text{RENi}_5$  group (RE – rare-earth) crystallize in a  $\text{CaCu}_5$ -type hexagonal crystal structure.<sup>1</sup> The effect of the crystalline electric field (CEF) dominates in this series, rather than exchange interactions, which are critical in materials containing rare-earth ions. At low temperatures, the  $\text{RENi}_5$  compounds are magnetically ordered, except for  $\text{PrNi}_5$  and  $\text{CeNi}_5$ .  $\text{PrNi}_5$  is a Van Vleck paramagnet, and due to the CEF splitting, the ground state of the lowest multiplet is a non-magnetic singlet separated from the first excited magnetic states by a relatively broad energy gap.<sup>2</sup> The  $\text{CeNi}_5$  is a Stoner enhanced paramagnet, and it is well-known that, in this compound, the influence of spin fluctuations was observed on its transport properties. This means that the temperature dependence of the magnetic susceptibility does not follow the Curie-Weiss law but shows a wide maximum around 100 K. It was observed that Ce is non-magnetic in  $\text{CeNi}_5$ . The above-mentioned

maximum at  $\chi(T)$  originates from the thermal smearing of the  $d$ -electron density of states at the Fermi level, which is enhanced by spin fluctuations,<sup>3,4</sup> and the Ce ions are still in a  $4^+$  valence state. In these intermetallic compounds' Ni is non-magnetic, but it is very close to the onset of magnetism.<sup>5</sup> Moreover,  $\text{GdNi}_5$  is known as a ferromagnetic compound with  $T_c = 32$  K.<sup>6,7</sup> Some of the magnetic and thermodynamic properties of  $(\text{Ce,Gd})\text{Ni}_5$  have been studied.<sup>8</sup> The present research was undertaken to fabricate  $\text{Gd}_{1-x}\text{Ce}_x\text{Ni}_5$  ( $x = 0; 0.2; 0.5; 0.8$  and  $1$ ) melt-spun ribbons in order to experimentally assess their ground-state magnetic properties.

## II. EXPERIMENTAL DETAILS

First, approximately 5 g ingots with the composition of  $\text{Gd}_{1-x}\text{Ce}_x\text{Ni}_5$  ( $x = 0; 0.2; 0.5; 0.8$  and  $1$ ) were produced by arc-melting from highly pure constituents (Ce 99.99 mass %, Gd 99.6 mass % and Ni 99.999 mass %) in a stoichiometric ratio in a water-cooled Cu-hearth under purified argon atmosphere. To ensure its good

starting homogeneity, each one of the ingots was re-melted three times; the final mass of the as-cast ingot coincided with the starting one. The losses during sample preparation were present but very small, around 0.6%, to conclude that we could make a very good synthesis. These samples were obtained in the form of melt-spun ribbons flakes under a highly pure He atmosphere at a linear speed of the rotating copper wheel of 25 m/s in an Edmund Bühler model SC melt spinner system.

The X-ray diffraction (XRD) pattern of finely powdered melt-spun ribbons was recorded between  $20^\circ$  and  $100^\circ$  with a  $2\theta$  increment of  $0.02^\circ$  in a high-resolution Bruker D8 Advance diffractometer with a wavelength of 0.15418 nm corresponding to Cu  $K\alpha$  radiation. A dual-beam scanning electron microscope (SEM) TESCAN Vega 3 XMU was used to obtain secondary electron images of the microstructure, and the system was equipped with an energy dispersive spectroscopy (EDS) detector.

The magnetic measurements were carried out using a 9 T Quantum Design Dynacool<sup>®</sup> Physical Property Measurement System (PPMS) using the vibrating sample magnetometer option. Measurements were done on a needle-like ribbon samples applying the external magnetic field through the central length of ribbon axis (coincident with the rolling direction) to reduce the effect of the internal demagnetizing field. The temperature dependences of the

magnetization, the  $M(T)$  curves, were measured under static magnetic fields with a sweeping rate of 2 K/min. The specific heat,  $C_p$ , was measured as a function of temperature using the heat capacity module of a Quantum Design Evercool-I<sup>®</sup> PPMS<sup>®</sup> system; this option measures the thermal response of a small thin sample using a thermal-relaxation calorimeter.

### III. RESULTS AND DISCUSSION

Fig. 1(a)-(c) shows the experimental X-ray powder diffraction patterns for some chosen examples and their Rietveld refinements achieved with the FULLPROF suite package.<sup>9</sup> The figure shows that all the Bragg diffraction reflections were correctly identified and indexed based on the hexagonal  $CaCu_5$  crystal structure (space group  $P6/mmm$ ), and the Vegard law can be applied. The determined lattice parameters are reasonably in agreement with the reported ones in the literature for the bulk alloys located at both ends of the series.<sup>8</sup> Thus, the employed processing technique simplifies the fabrication procedure in the sense that it circumvents the long-term high-temperature thermal annealing usually used to produce single-phase alloys prepared by a conventional melting process, which agrees with the SEM observations.

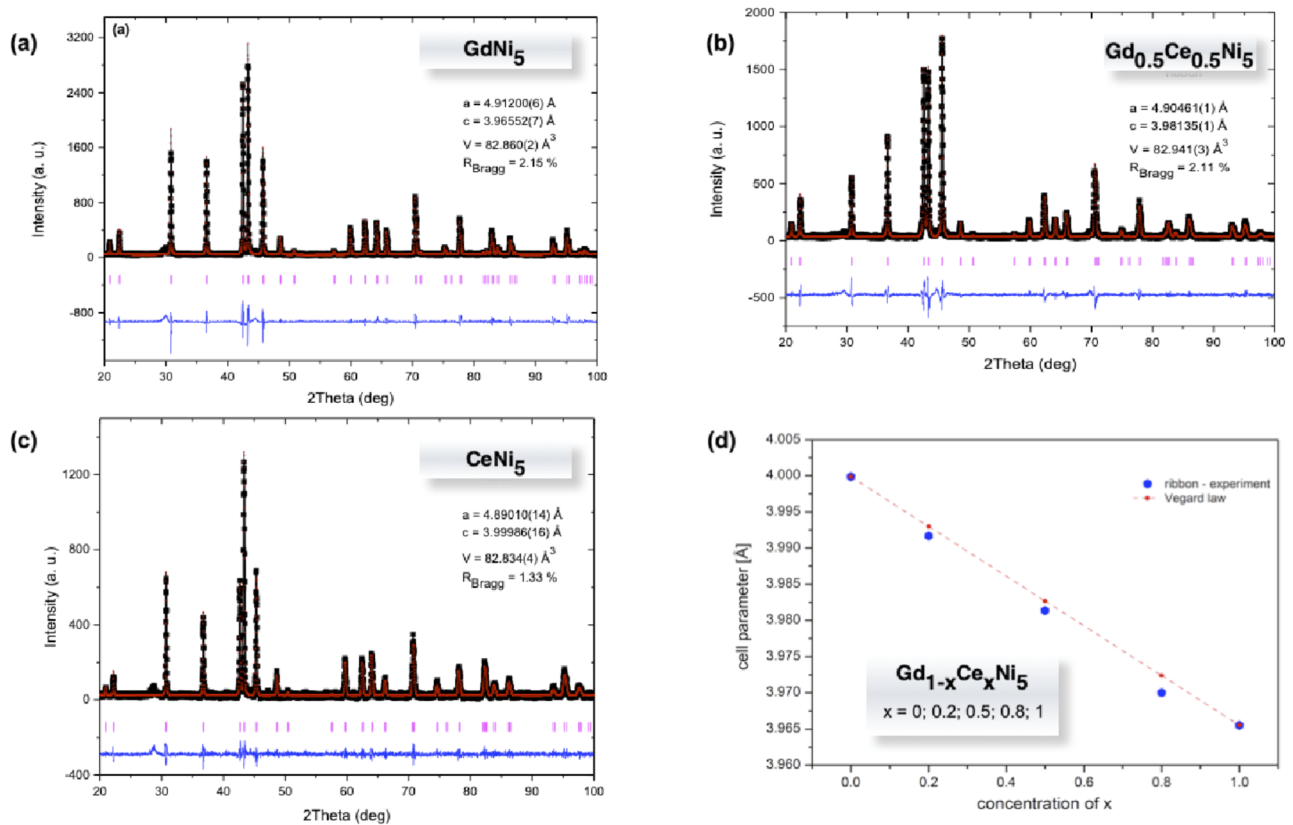


**FIG. 1.** (a)-(c) Experimental data and Rietveld refinement of the room temperature X-ray powder diffraction patterns of  $Gd_{1-x}Ce_xNi_5$  ( $x = 0; 0.2; 0.5; 0.8$  and  $1$ ) melt-spun ribbons. (d) Evolution of the obtained cell parameters in comparison with Vegard's law.

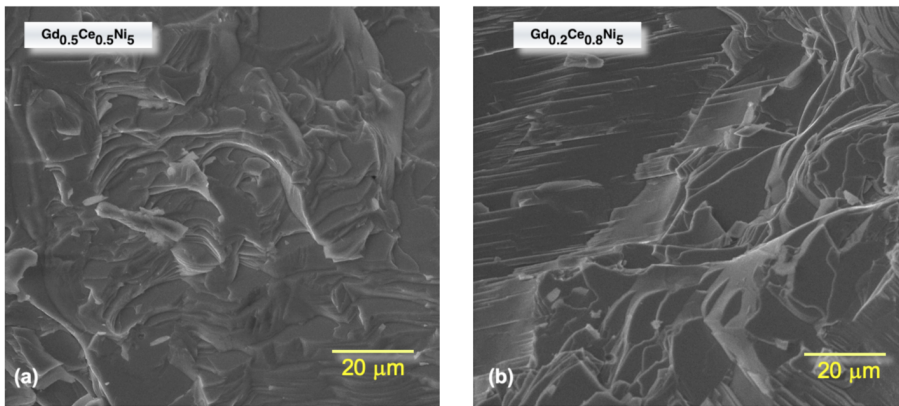


FIG. 2. (a)-(b) SEM micrographs showing the typical microstructure of ribbons.

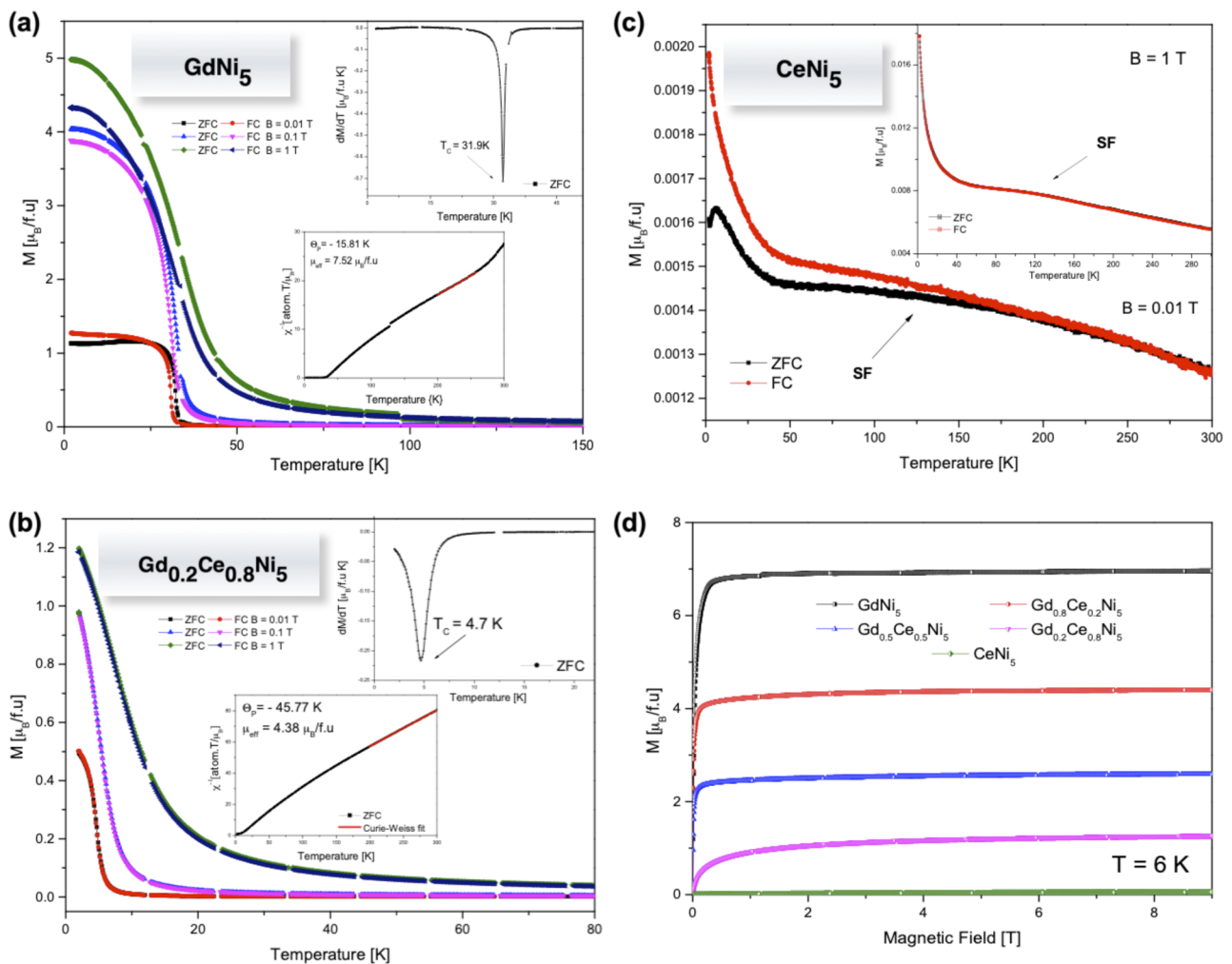


FIG. 3. (a)-(b) Temperature dependence of the magnetization at low- and high magnetic fields for  $GdNi_5$  and  $Gd_{0.2}Ce_{0.8}Ni_5$  samples. The inset (up) shows the  $dM/dT$  with the calculation of  $T_c$ . The inset (down) shows the inverse of the magnetic susceptibility fitted to a Curie-Weiss law. (c) Temperature dependence of the ZFC-FC magnetization at two different applied magnetic fields for  $CeNi_5$ , where a maximum ( $\sim 100$  K), connected with spin fluctuations effect is visible. (d) Characteristic behavior of the magnetic field dependence at very low temperatures of the magnetization for the whole studied series of ribbons.

**TABLE I.** Summary of the experimental values determined for  $\text{Gd}_{1-x}\text{Ce}_x\text{Ni}_5$  ( $x = 0; 0.2; 0.5; 0.8$  and  $1$ ): the transition temperature  $T_c$ , the paramagnetic Curie temperature  $\theta_p$ , the effective moment  $\mu_{\text{eff}}$  and the Sommerfeld coefficient  $\gamma$ .

$x$	$x = 0$	$x = 0.2$	$x = 0.5$	$x = 0.8$	$x = 1$
$T_c$ [K]	31	29	15.5	4.7	no observed
$\theta_p$ [K]	-15.81	38.5	-5.36	-45.77	-199.55
$\mu_{\text{eff}}$ [ $\mu_B/\text{f.u.}$ ]	7.52	7.03	4.57	4.38	3.52
$\gamma_{9T}$	32	30	16	9	no calculated

The typical SEM micrographs of the cross-section (fractured morphology), wheel surface of the synthesized quenched ribbons is shown in Fig. 2(a)-(b) for some chosen examples,  $\text{Gd}_{0.5}\text{Ce}_{0.5}\text{Ni}_5$  and  $\text{Gd}_{0.2}\text{Ce}_{0.8}\text{Ni}_5$ , of this series. Ribbons are polycrystalline and very fragile, with an average thickness of  $\approx 15 \mu\text{m}$ . At the ribbon surface that makes contact with the Cu wheel during the fabrication, the much faster cooling rate forms a thin layer of the texture layer.

The peaks grow through that thicker region whose longer axis tends to be aligned perpendicular to the ribbon surface (i.e., along the thermal gradient during solidification). If true that the preferred grain orientation is far from being perfect, it is a signature of some crystallographic texture in the synthesized ribbon samples. The fractured cross-section of many ribbon samples was observed, confirming this regularity. From more than 10 EDS spectra (not shown) collected from the ribbons surface, it was determined that within the experimental error (0.2 at. %), the elemental chemical composition of the prepared ribbons is close enough to the nominal one.

The temperature dependence of the magnetization at low- and high magnetic fields is presented in Fig. 3(a)-(b) again for some selected representatives' compounds. The low magnetic field curves for both samples, resp. for all compounds except  $\text{CeNi}_5$  unveil that the materials undergo a single well-defined magnetic order phase

transition. The Curie temperature  $T_c$  was obtained from the minimum of the first derivative of the  $M(T)$  curve (displayed in the inset on the top) in the phase transition region. The second insets display a Curie-Weiss fits in the high-temperature range. The effective paramagnetic moments  $\mu_{\text{eff}}$  and the paramagnetic Curie temperatures  $\theta_p$  obtained from the Curie-Weiss fits are presented in Table I. These results show that, with the increase of the Ce content  $T_c$  and  $\mu_{\text{eff}}$  decrease.

Another situation is described in Fig. 3 (c) where the  $M(T)$  curve is plotted for  $\text{CeNi}_5$ . A broad maximum of around 100 K followed by an increase of susceptibility at a lower temperature, is evident for both the low and high applied magnetic fields. The interpretation is double: some authors are inclined to believe that these tails at lower temperatures are intrinsic as signs to be on the verge of ferromagnetism,<sup>10,11</sup> and on the other hand, it is known that even a small concentration of magnetic impurities can cause such an upturn. Previous experimental studies on a bulk sample of  $\text{CeNi}_5$ <sup>4,12</sup> do not show any sign of low-temperature upturns in the susceptibility measurements, whereas a slight upturn is evident in Fig. 3 (c). This fact is an indication that the observed effects are not intrinsic but due to ferromagnetic impurities.<sup>11</sup> However, they are connected with the spin fluctuations effect, which agrees with the authors' explanation in Ref. 13. The isothermal magnetization as a function of the applied magnetic field, at  $T = 6$  K, is plotted in Fig. 3 (d). The  $\text{Ce}^{3+}$  ion has a smaller contribution to the total magnetization than  $\text{Gd}^{3+}$ . Due to the sample preparation process, the anisotropy is lower in general for ribbons.<sup>6,8</sup>

The specific heat analysis is plotted in Fig. 4(a) for the  $\text{Gd}_{0.5}\text{Ce}_{0.5}\text{Ni}_5$  compound as an example of the studied series. The measurements show typical metallic behavior, and in a high temperature range, they follow Dulong-Petit law for all samples. The corresponding calculation of the phonon contribution and  $4f$  contributions ( $C_{4f}$ ) to the heat capacity is also presented, and the same analysis was done for all samples. At zero applied magnetic field,  $C_{4f}$  is dominated by a  $\lambda$ -like anomaly at  $T_c = 15.5$  K. From the  $C(T)/T$  vs  $T^2$  dependences (not shown), the electronic Sommerfeld  $\gamma$

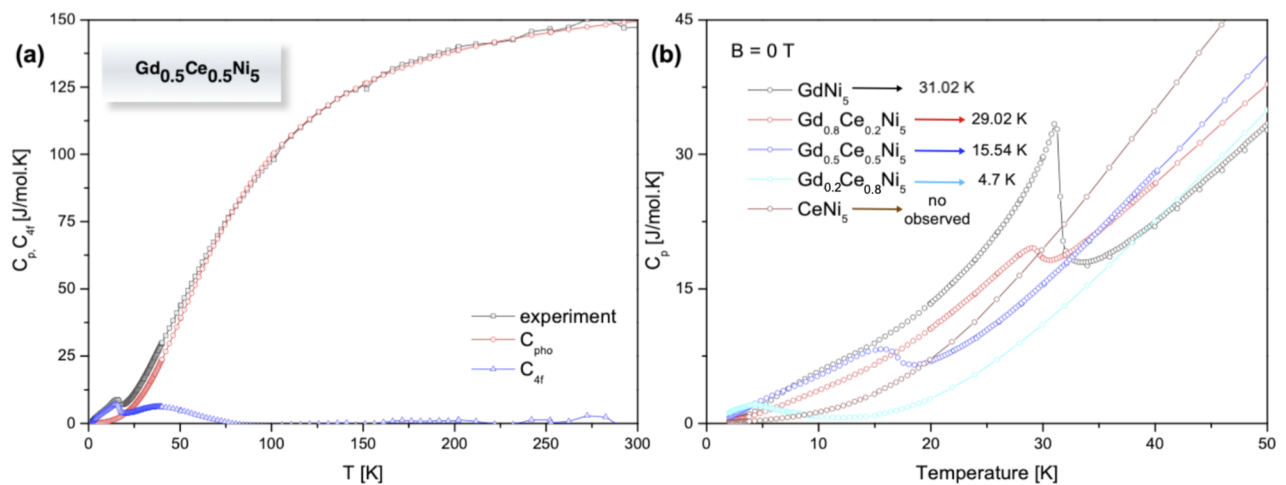


**FIG. 4.** (a)  $C_p(T)$  measured and calculated contributions to the total specific heat for  $\text{Gd}_{0.5}\text{Ce}_{0.5}\text{Ni}_5$ . (b) Low-temperature detail of the specific heat for all compositions with no applied magnetic field, where the transition temperatures are more visible.

coefficient was determined, and it is reported in Table I. The magnetic contribution is significant at zero applied magnetic field, so the data at the applied magnetic field of 9 T were used for this purpose.

Moreover, there is not a heavy-fermion behavior in this system. The temperature behavior of all the studied ribbon samples is compared in Fig. 4(b). It is evident that, increasing the Ce content, the position of low-temperature anomaly decreases. As it was expected, CeNi<sub>5</sub> has no magnetic ordering down to very low temperatures. The conclusion is that the substitution of Gd with Ce tends to suppress magnetic ordering.

#### IV. CONCLUSIONS

To sum up, we have evidence that through the melt-spinning technique, we were able to produce single phase melt-spun ribbons with the CaCu<sub>5</sub>-type hexagonal crystal structure of the Gd<sub>1-x</sub>Ce<sub>x</sub>Ni<sub>5</sub> (x = 0, 0.2, 0.5, 0.8 and 1) series, with similar structural and magnetic properties than the corresponding bulk polycrystalline compounds. The effect of Ce doping is to suppress the magnetic transition, and CeNi<sub>5</sub> is distinguished by the spin fluctuations effect observed around 100 K. So, in the future will be worth to calculate the magnetocaloric effect. In order to determine more precisely the Sommerfeld coefficients without being affected by the magnetic contribution, it is necessary to measure the heat capacity below 2 K.

#### ACKNOWLEDGMENTS

This research work was supported partially by VEGA 1/0404/21; VEGA 1/0705/20; VEGA 1/0053/19, and APVV-16-0079.

#### AUTHOR DECLARATIONS

##### Conflict of Interest

The authors have no conflicts to disclose.

#### DATA AVAILABILITY

The data that support the findings of this study are available from the corresponding author upon reasonable request.

#### REFERENCES

- <sup>1</sup>M. Reiffers, J. A. Blanco, J. I. Espeso, J. García Soldevilla, H. J. H. Smilde, and J. C. Gómez Sal, *Solid State Commun.* **103**, 179 (1997).
- <sup>2</sup>A. S. Ermolenko, A. V. Korolev, and G. V. Ivanova, *Phys. Metal. Metallography* **109**(4), 358–365 (2010).
- <sup>3</sup>M. Reiffers, M. Della Mea, E. Bauer, and G. Pristáš, *J. Magn. Mater.* **272–276**, 605 (2004).
- <sup>4</sup>D. Gignoux, F. Givord, R. Lemaire, and F. Tasse, *J. Phys.* **43**, C7-257 (1982).
- <sup>5</sup>V. M. T. S. Barthem, D. Gignoux, A. Naït-Saada, D. Schmitt, and G. Creuzet, *Phys. Rev. B* **37**, 1733 (1988).
- <sup>6</sup>F. Kayzel, *Magnetic and Thermodynamic Properties of RNi<sub>5</sub> Compounds* (Amsterdam, 1994).
- <sup>7</sup>A. Bajorek, G. Chelkowska, and B. Andrzejewski, *J. Alloy Compounds* **509**(3), 578–584 (2011).
- <sup>8</sup>A. Dzubinska, M. Reiffers, J. I. Espeso, and J. Rodríguez Fernández, *Acta Physica Polonica A* **131**(4), 997–999 (2017).
- <sup>9</sup>J. Rodríguez-Carvajal, *Physica B* **192**, 55 (1993).
- <sup>10</sup>J. Tang, L. Li, C. J. O'Connor, and Y. S. Lee, *J. Alloys Compounds* **207–208**, 241 (1994).
- <sup>11</sup>S. Nasu, H. H. Neumann, N. Marzouk, R. S. Craig, and W. E. Wallace, *J. Phys. Chem. Solids* **32**, 2779 (1971).
- <sup>12</sup>O. Musil, P. Svoboda, M. Diviš, and V. Sechovský, *Czech. J. Phys.* **54**, 311 (2004).
- <sup>13</sup>M. Zapotoková, I. Čurlik, M. Giovannini, and M. Reiffers, *Europ. Phys. J. B* **86**, 129 (2013).